



## Catalytic upgrading of biomass pyrolysis vapors and model compounds using niobia supported Pd catalyst



Camila A. Teles<sup>a,b</sup>, Priscilla M. de Souza<sup>a,1</sup>, Raimundo C. Rabelo-Neto<sup>a</sup>, Michael B. Griffin<sup>c</sup>, Calvin Mukarakate<sup>c</sup>, Kellene A. Orton<sup>c</sup>, Daniel E. Resasco<sup>d</sup>, Fábio B. Noronha<sup>a,b,\*</sup>

<sup>a</sup> National Institute of Technology, Catalysis Division, Rio de Janeiro, 20081-312, Brazil

<sup>b</sup> Military Institute of Engineering, Chemical Engineering Department, Praça Gal. Tibúrcio 80, Rio de Janeiro, 22290-270, Brazil

<sup>c</sup> National Bioenergy Center, National Renewable Energy Laboratory, Golden, CO, 80405, USA

<sup>d</sup> Center for Biomass Refining, School of Chemical, Biological and Materials Engineering, The University of Oklahoma, Norman, OK, 73019, USA

### ARTICLE INFO

**Keywords:**  
Biomass  
Pyrolysis  
HDO  
Model molecules  
 $\text{Nb}_2\text{O}_5$

### ABSTRACT

This work addresses the effect of the support on the performance of Pd-based catalysts for hydrodeoxygenation of different model molecules (phenol, m-cresol, anisole, guaiacol) in the vapor phase at 573 K. The activity and the selectivity to deoxygenated products strongly depended on the support, regardless the model molecule. For HDO of phenol and m-cresol, benzene and toluene were the dominant products on niobia supported catalysts, whereas cyclohexanone and methylcyclohexanone were the main compounds formed on Pd/SiO<sub>2</sub>. For HDO of anisole, demethylation reaction producing benzene is favored over Pd/Nb<sub>2</sub>O<sub>5</sub> catalyst, while demethylation is the preferred route over Pd/SiO<sub>2</sub>. Phenol and methanol were the main products observed for HDO of guaiacol over all catalysts but significant formation of benzene was detected over Pd/Nb<sub>2</sub>O<sub>5</sub>. The improved deoxygenation performance over the niobia supported catalysts is explained in terms of the oxophilic sites represented by Nb<sup>4+</sup>/Nb<sup>5+</sup> cations. These catalysts were also tested for HDO of pine pyrolysis vapors. All three catalysts were effective for reducing the total yield of oxygenated products. The extent of deoxygenation was highest over the Pd/Nb<sub>2</sub>O<sub>5</sub> and Pd/NbOPO<sub>4</sub> catalysts. The effectiveness of Pd/Nb<sub>2</sub>O<sub>5</sub> and Pd/NbOPO<sub>4</sub> for deoxygenation of real feeds is in good agreement with the model compound results and suggests that these catalysts are promising materials for the upgrading of pyrolysis vapors to produce hydrocarbon fuels.

### 1. Introduction

The fast pyrolysis of lignocellulosic biomass produces bio-oil, a complex mixture of several organic compounds such as acids, alcohols, ketones, aldehydes, phenols, sugars, furans and oligomers [1]. Bio-oil has been identified as an attractive source towards the sustainable production of biofuels and chemicals. However, this liquid has poor quality and is thermally and chemically unstable due to its high content of water and oxygenated species. Consequently, bio-oil must be upgraded to be used as a fuel in combustion engines. The catalytic hydrodeoxygenation (HDO) of bio-oil is considered a promising technology for bio-oil upgrading, in which molecularly bound oxygen is removed in the presence of hydrogen and a catalyst [2].

There are three different process configurations for the upgrading of pyrolysis oil. The first configuration involves non-catalytic fast pyrolysis followed by condensation and hydrotreating of the products at

high pressure in a down-stream reactor [3]. This process is the most widely used. However, the condensed bio-oil produced is highly unstable and a two-step hydrotreating process is required. Other options include in situ and ex situ catalytic fast pyrolysis, in which vapor phase catalytic upgrading occurs either within the pyrolysis reactor or in a second down-stream reactor, respectively. These technologies offer the advantage of oxygen removal prior to condensation and immediate stabilization of the product mixture.

There are only few reports in the literature about the HDO of biomass fast pyrolysis vapors at atmospheric pressure. Zeolite (HZSM-5), metal oxides (MoO<sub>3</sub>) and supported metals (Ru/TiO<sub>2</sub>) are among the catalysts which have been investigated [3–7]. Note et al. [5] carried out the HDO of cellulose, lignin and corn stover pyrolysis vapors over a MoO<sub>3</sub> catalyst, using a hydropyrolyzer coupled to a fixed-bed reactor operated at 400 °C. The main products were linear alkanes (C<sub>1</sub> to C<sub>6</sub>) and aromatics, which comprised approximately 75–90 % of the

\* Corresponding author at: National Institute of Technology, Catalysis Division, Rio de Janeiro, 20081-312, Brazil.  
E-mail address: [fabio.bellot@int.gov.br](mailto:fabio.bellot@int.gov.br) (F.B. Noronha).

<sup>1</sup> Present address: Federal University of Rio de Janeiro, Chemical Engineering Program, Rio de Janeiro, 21941-972, Brazil.

volatile pyrolysis products (excluding char) for the three feedstocks. A high selectivity to deoxygenated aromatic species was also reported for the HDO of pine pyrolysis vapors over fresh  $\text{MoO}_3/\text{TiO}_2$  and  $\text{MoO}_3/\text{ZrO}_2$ . However, the yield of deoxygenated products decreased as the catalysts were exposed to increasing amounts of biomass, which was attributed to deactivation from coking. Zu et al. [7] studied the catalytic upgrading of biomass (poplar) fast pyrolysis vapors over  $\text{TiO}_2$ ,  $\text{TiO}_2\text{-ZrO}_2$ ,  $\text{CeO}_2/\text{TiO}_2$ ,  $\text{CeO}_2/\text{TiO}_2\text{-ZrO}_2$  in the absence of metals and after being impregnated with Pd or Ru. The titania supported catalysts converted the lignin-derived oligomers into monomeric phenols and reduced the concentration of aldehydes and sugars. The  $\text{TiO}_2\text{-ZrO}_2$  supported catalysts decreased the formation of phenols and acids and increased the concentration of hydrocarbons, light linear ketones and cyclopentanones.

However, the development of a stable catalyst that can selectively remove the oxygenated groups with low hydrogen consumption is still a challenge and the design of a proper catalyst for HDO requires a detailed knowledge of the reaction mechanism. Due to the complex chemical composition of bio-oil, model molecules that are representatives of families of compounds derived from biomass have been studied. For instance, the lignin fraction of lignocellulosic biomass is a polymer with complex structure that is composed of three monomers namely coniferyl, p-coumaryl and sinapyl alcohol and these monomers are connected through different alkyl, aryl and ether linkages. These monomers contain different functional groups bonded to the aromatic ring such as hydroxyl or methoxy. The coumaryl alcohol has one hydroxyl group on the aromatic ring whereas coniferyl and sinapyl alcohol has one and two methoxy groups, respectively. Lignin decomposition by fast pyrolysis produces a mixture of phenolics compounds that may contain methoxy groups and even phenolic oligomers (dimers, trimers and tetramers). Therefore, the use of lignin model compounds as a representative for lignin has been preferred for the fundamental studies because they allow the interpretation and understanding of mechanism and kinetics and the understanding of the role of heterogeneous catalyst components.

There are a number of model compounds that can mimic the structure of lignin such as phenol, cresol, anisole or guaiacol. These compounds contain different functional groups on the aromatic ring such as hydroxyl or methoxy groups.

For instance, the HDO of m-cresol [8–11], and phenol [12–19] was performed over different metals (Pd, Pt, Ru, Rh, Ni, Co, Fe, NiFe) and supports (C,  $\text{SiO}_2$ ,  $\text{Al}_2\text{O}_3$ ,  $\text{TiO}_2$ ,  $\text{ZrO}_2$ ,  $\text{CeO}_2$ ,  $\text{CeZrO}_2$ ,  $\text{Nb}_2\text{O}_5$ ,  $\text{V}_2\text{O}_5$ ). From these studies, three reaction pathways have been proposed for the removal of hydroxyl group from phenol and cresol molecules [20]. The first one involves the sequential hydrogenation of the aromatic ring on metal sites followed by dehydration of cyclohexanol/3-methylcyclohexanol on acid sites. Therefore, this reaction pathway depends on the acidity of the support. The second route is the direct deoxygenation and involves the cleavage of the C–O bond in the phenolic molecule. This pathway requires a relatively high activation energy but it may occur on oxophilic metals such as Ru as well as supports like  $\text{TiO}_2$ , due to the strong interaction with the oxygen atom that reduces the energy barrier for the direct cleavage of the C–O bond of the aromatic ring. The last reaction pathway is based on the tautomerization of phenolic compound to a cyclohexadienone intermediate (2,4-cyclohexadienone or 3,5-methylcyclohexadienone). This intermediate may react by two different routes: (i) the hydrogenation of the ring, producing cyclohexanone/methyl-cyclohexanone and cyclohexanol/methyl-cyclohexanol; or (ii) hydrogenation of the carbonyl group, leading to the formation of benzene or toluene.

The HDO reaction of anisole [21–23] and guaiacol [24–26] has been also extensively studied over different catalysts in the literature. These studies revealed that the type of the metal and support plays a key role on the deoxygenation activity. However, there is not a systematic study about the effect of the support on the activity for removal of different functional groups in the same series of catalysts. Furthermore, the

majority of the studies used only model compounds but they did not test the developed catalyst under a real feed in order to correlate the performance of the catalyst under HDO of model molecules and HDO of a bio-oil.

Therefore, the aim of this work is to study the effect of the type of support ( $\text{SiO}_2$  and  $\text{Nb}_2\text{O}_5$ ) on the deoxygenation activity of Pd-based catalysts for the removal of different oxygenated functional groups: hydroxyl (phenol and m-cresol), methoxy (anisole) and hydroxyl and methoxy groups in the same molecule (guaiacol). The mechanism for the HDO reaction of the different molecules is discussed. Finally, these catalysts are tested on the upgrading of biomass pyrolysis vapors.

## 2. Experimental section

### 2.1. Catalyst preparation

$\text{SiO}_2$ ,  $\text{NbOPO}_4$  and  $\text{Nb}_2\text{O}_5$  were used to prepare supported Pd catalysts.  $\text{SiO}_2$  (silica gel, Aldrich, 7631-86-9) was calcined under air flow (50 mL/min) at a heating rate of 5 K/min up to 1073 K, remaining at this temperature for 5 h.  $\text{Nb}_2\text{O}_5$  was obtained by calcination of niobic acid (CBMM) under air flow (50 mL/min) at 5 K/min up to 673 K for 4 h.  $\text{NbOPO}_4$  was also provided by CBMM and underwent the same calcination procedure described for the preparation of  $\text{Nb}_2\text{O}_5$ . Pd catalysts were prepared by incipient wetness impregnation of the support with an aqueous solution of  $\text{Pd}(\text{NO}_3)_2\cdot 2\text{H}_2\text{O}$  (solution of 20% Pd in nitric acid, Umicore) to obtain 2 wt% of Pd. After impregnation, the powder was dried in air at 293 K for 12 h and then calcined under synthetic air flow (50 mL/min) at 673 K for 3 h (2 K/min). Then, the samples were sieved between 150–270 mesh.

### 2.2. Catalyst characterization

Specific surface areas of the samples were measured on a Micromeritics ASAP 2020 analyzer by  $\text{N}_2$  adsorption at 77 K. The nature of acid sites was determined by DRIFTS of adsorbed pyridine using a Nicolet Nexus 870 instrument with a DTGS-TEC detector and a Thermo Spectra-Tech reaction chamber with ZnSe windows. The samples were previously reduced under  $\text{H}_2$  at 573 K for a period of 1 h. Then, the temperature was decreased to 373 K and He was flowed through the sample, which was followed by the record of a spectrum that was used as a background. Pyridine adsorption was carried out by bubbling He (30 mL/min) through a saturator for 30 min, followed by a He purge. Absorption spectra were recorded at a resolution of  $4 \text{ cm}^{-1}$ , accumulating 256 scans. Then, the temperature was raised to 423, 523 and 623 K and spectra were obtained. The density of acid sites of the catalysts was measured by temperature-programmed desorption of ammonia ( $\text{NH}_3\text{-TPD}$ ). The samples (400 mg) were reduced under a flow of 60 mL/min of a mixture 10%  $\text{H}_2/\text{He}$  at a heating rate of 10 K/min up to 573, for 1 h, and then purged in He flow (30 mL/min) for 30 min. After reduction, the sample was cooled to 423 K and the feed composition was switched to a mixture containing 4%  $\text{NH}_3$  in He (30 mL/min) for 30 min. The physisorbed ammonia was flushed out with flowing He (30 mL/min) for 1 h. Then, the catalyst was heated under He at 20 K/min to 773 K.

In situ X-Ray powder diffraction (XRD) measurements were performed at the beamline XRD1-D12A [27] of the Brazilian Synchrotron Light Laboratory (LNLS), Campinas, Brazil. The sample was loaded into a quartz capillary of 1.0 mm diameter between two quartz wool beds. The capillary was placed in a reaction cell connected to a 3-circle Heavy Duty diffractometer from Newport® and oriented horizontally and perpendicularly to the X-ray beam. A Yaskawa-Motoman robotic arm was used to hold a hot air blower above the sample to control the temperature during the experiment. The diffraction patterns in a  $2\theta$  range between 10 and  $120^\circ$  with an acquisition time of 150 s were obtained using an array of 24 Mythen (Dectris®), installed in the delta circle at 760 mm from the sample. The wavelength of  $\lambda = 1.0332 \text{ \AA}$  was

selected by a double-crystal Si (111) monochromator.  $\lambda$  and the distance of the sample to the detector were calibrated using Si (SRM 640d) and  $\text{Al}_2\text{O}_3$  (SRM 676a) powders NIST standards. The measurements were carried out while the sample underwent the following treatments: (i) under a flow of He (8 mL/min) at 298 K; (ii) under a flow of pure  $\text{H}_2$  (8 mL/min) at 298 K, and (iii) under a flow of pure  $\text{H}_2$  (8 mL/min) from 298 to 573 K at a heating of 10 K/min, remaining at this temperature for 1 h. The average crystallite size of metallic Pd under different treatments was calculated using the Scherrer equation and the line characteristic of  $\text{Pd}^\circ$  (111) at  $2\theta = 26.5^\circ$ .

The dehydrogenation of cyclohexane was used as an insensitive structure reaction to determine the metal dispersion of supported Pd catalysts [28,29]. For  $\text{Pd}/\text{Nb}_2\text{O}_5$  catalyst, the determination of Pd particle size by transmission electron microscopy (TEM) is challenging due to the low contrast between the Pd and  $\text{Nb}_2\text{O}_5$  support. Therefore, the Pd dispersion was determined by a correlation between the rate of cyclohexane dehydrogenation and palladium dispersion of catalysts ( $\text{Pd}/\text{SiO}_2$ ,  $\text{Pd}/\text{Al}_2\text{O}_3$  and  $\text{Pd}/\text{ZrO}_2$ ) with dispersion measured by CO chemisorption.

This procedure enables the measurement of the Pd dispersion of fresh and used catalysts (after HDO of phenol for 22 h). A fixed-bed reactor was used to carry out the dehydrogenation of cyclohexane reaction over fresh and used catalysts. The fresh samples (60 mg) were first reduced at 573 K for 1 h and then cooled to the cyclohexane dehydrogenation reaction temperature (543 K). The reaction mixture ( $\text{WHSV} = 23 \text{ h}^{-1}$ ) was fed into the reactor after bubbling  $\text{H}_2$  through a saturator containing cyclohexane maintained at 285 K ( $\text{H}_2/\text{C}_6\text{H}_{12} = 13.2$ ). For the used catalysts, after HDO of phenol or guaiacol for 22 h, the saturator containing the model compound was bypassed and hydrogen was allowed to flow through the catalyst for 30 min at 573 K, which removed hydrocarbons that remained adsorbed on the surface as well as any carbonaceous deposited present. The reactor was cooled to 543 K under hydrogen. Then, a cyclohexane/ $\text{H}_2$  mixture was passed through the reactor. The effluent was analyzed by GCMS Agilent 7890 A/5975C.

Temperature-programmed oxidation (TPO) experiments were carried out to investigate the formation of carbon after the HDO of phenol and guaiacol during 22 h of TOS. TPO experiments were carried out in a micro-reactor coupled to a quadrupole mass spectrometer (Gas analysis – Prisma QME200 / Pfeiffer). Two types of experiments were carried out. In the first, after reaction, the reactor temperature was kept at 573 K and flushed in He for 30 min and then cooled to room temperature. Then, the samples were heated at a rate of 10 K/min in a 20%  $\text{O}_2$ :He mixture (30 mL/min) up to 1173 K. In the other experiment, phenol or guaiacol were adsorbed on the surface of the catalyst bubbling He through a saturator containing phenol or guaiacol and then, the TPO experiment was performed at the same conditions previously described.

### 2.3. HDO of model molecules

Phenol (99 wt%), anisole (99 wt%), m-cresol (99 wt%) and guaiacol (98 wt%) obtained from Sigma-Aldrich were used as feeds in the hydrodeoxygenation reaction. The catalytic experiments were conducted in a vapor-phase fixed-bed flow reactor system, operating at atmospheric pressure of  $\text{H}_2$  and 573 K. Preliminary calculations (Supplementary Information) and tests were carried out following the same criteria proposed by Madon and Boudart (1982) to ensure that internal and external mass transfer limitations were eliminated [30]. Depending on the molecule used, the reactant mixture was obtained or by saturator (phenol, guaiacol) or by syringe pump (anisole, m-cresol). In general, the carrier gas flow rate was 60 mL/min of  $\text{H}_2$  and the resultant  $\text{H}_2$ /model compound molar ratio was 51 for m-cresol (0.0184 atm), 53 for anisole (0.0190 atm) and 60 for phenol and guaiacol (0.0157 atm). The catalysts (53–106  $\mu\text{m}$  size range) were diluted with inert material ( $m_{\text{inert}}/m_{\text{cat}} = 3$ ) and packed in the reactor

between two layers of quartz wool. Prior to reaction, the catalyst was reduced in situ under pure hydrogen (60 mL/min) at 573 (10 K/min) for 1 h. Two different series of experiments were performed to determine the initial phenol conversion and to study catalyst deactivation. In the first series, each catalyst was tested at various W/F values by changing the amount of the catalyst (3 to 90 mg) and WSHV (2 to  $62 \text{ h}^{-1}$ ) in order to obtain low conversion (around 10%) for all reactions. W/F is defined as catalyst mass (g) divided by mass flow rate (g/h) of the organic feed. The initial phenol conversion was taken after 5 min of TOS in order to avoid catalyst deactivation. In the second series, 60–120 mg of catalyst and a total flow rate of  $60 \text{ mL}\cdot\text{min}^{-1}$  were used for all catalysts in order to observe catalyst deactivation within 22 h TOS. To avoid condensation, all lines were heated at (523 K). The reaction products were analyzed by GCMS Agilent 7890 A/5975C, using HP-Innowax capillary column and a flame-ionization detector (FID). The product yield and selectivity for each product were calculated as follows:

$$\text{yield (\%)} = \frac{\text{mol of product}}{\text{mol of organic fed}} \times 100 \quad (1)$$

$$\text{Selectivity (\%)} = \frac{\text{mol of product}}{\text{mol of organic consumed}} \times 100 \quad (2)$$

### 2.4. HDO of pine pyrolysis vapors

A tandem micropyrolyzer-GCMS system (py-GCMS) was used to identify and quantify products from the catalytic upgrading of pine pyrolysis vapors. The system has been described previously [31]. Briefly, it consists of a micropyrolyzer (Rx-5030TR, Frontier Laboratories, Japan) coupled to an autosampler (AS-1020E), a microjet cryo-trap (MJT-1030Ex) and a GCMS (7890B/5977 A, Agilent Technologies). The micropyrolyzer has two vertical heating zones in series: one for pyrolysis and one for upgrading of the pyrolysis vapours. Helium (54 mL/min) was used as the carrier gas in the pyrolysis zone, and  $\text{H}_2$  (54 mL/min) was introduced prior to the upgrading zone. The temperatures of pyrolysis and upgrading zones were maintained at 773 K and 673 K, respectively. Prior to reaction testing, each catalyst was reduced in flowing 50%  $\text{H}_2$ /He at 573 K for 0.5 h. Biomass was introduced by using the autosampler to insert stainless steel boats containing 0.5 mg of pine into the pyrolysis zone. A continuous flow of He was utilized to sweep the pyrolysis vapors over a fixed bed containing 10 mg of catalyst and 10 mg sand supported on a plug of quartz wool. Data represent the average of nine vapor pulses collected over three separate catalyst charges and error bars represent  $\pm \sigma/2$ . Carbon yield was calculated according to the following equation:

$$C_{\text{yield}} = \frac{\sum_j m_j [C]_j}{m_f [C]_f} \times 100 \quad (3)$$

Where  $j$  = product  $j$ ,  $[C]_j$  = C content of product  $j$ , g C/g product  $j$ ,  $[C]_f$  = C content of feed, g C/g feed,  $m_j$  = mass of product  $j$ , g product  $j$ ,  $m_f$  = mass of feed, g feed

The upgraded vapours were collected by the microjet cryo-trap, which was maintained at 77 K. Every ca. 30 min, the vapors were rapidly injected into the capillary column of the GCMS. Products were identified using a mass spectrometer through comparison with known standards and a NIST library. Products were quantified using an FID, with the exception for  $\text{CO}_2$  and CO, which were quantified using the MS and TCD, respectively. Response factors were developed using standards containing 25 representative compounds (8 aromatic hydrocarbons, 10 oxygenates, 5 olefins, 6 alkanes, and CO and  $\text{CO}_2$ ). In the case that standards were not available, response factors were estimated based on compound with similar chemical composition and molecular weight.

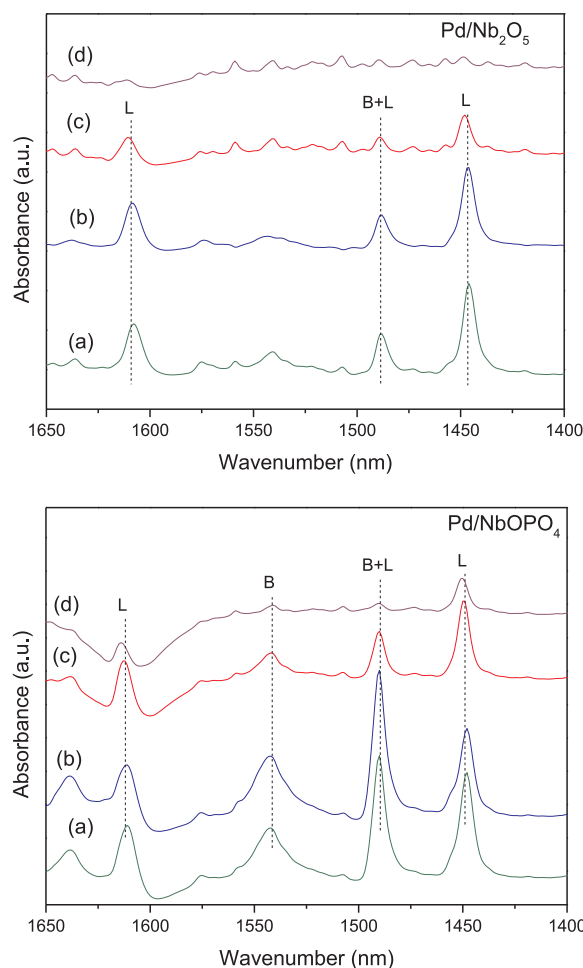


**Fig. 1.** DRIFT spectra of pyridine chemisorption at (a) 373 K and pyridine desorption at (b) 423 K, (c) 523 K and (d) 623 K for Pd/Nb<sub>2</sub>O<sub>5</sub> and Pd/NbOPO<sub>4</sub> catalysts reduced at 573 K. (L) Lewis acid sites; (B) Brønsted acid sites.

### 3. Results and discussion

#### 3.1. Catalyst characterization

The BET surface areas of the catalysts were 153 (Pd/SiO<sub>2</sub>), 122 (Pd/NbOPO<sub>4</sub>) and 87 m<sup>2</sup>/g (Pd/Nb<sub>2</sub>O<sub>5</sub>). Fig. 1 shows the DRIFTS spectra of adsorbed pyridine over niobia supported catalysts. No bands were detected on the spectra of Pd/SiO<sub>2</sub>. The infrared spectrum after pyridine adsorption on Pd/Nb<sub>2</sub>O<sub>5</sub> catalyst showed bands at 1446, 1487, and 1607 cm<sup>-1</sup>, which corresponds to the vibrational mode of pyridine adsorbed on the Lewis acid sites (L) of the support represented by the uncoordinated Nb cations [32,33]. In addition to the bands corresponding to Lewis acid sites, the DRIFTS spectrum of pyridine adsorbed on Pd/NbOPO<sub>4</sub> also exhibits bands attributed to Brønsted acid sites (B) (1542 cm<sup>-1</sup>) [32,33]. Increasing the temperature decreased the intensity of all bands in the DRIFTS spectra of adsorbed pyridine. This reduction was most significant on the Pd/Nb<sub>2</sub>O<sub>5</sub> catalyst, suggesting that acid site strength was lower over Pd/Nb<sub>2</sub>O<sub>5</sub> compared to Pd/NbOPO<sub>4</sub>.

The density of acid sites of the catalysts was determined by NH<sub>3</sub>-TPD. The TPD profiles of desorbed ammonia are shown in Fig. 2. The amount of ammonia desorbed on Pd/SiO<sub>2</sub> was negligible. The TPD profiles of Pd/Nb<sub>2</sub>O<sub>5</sub> and Pd/NbOPO<sub>4</sub> exhibit multiple peaks poorly resolved between 300 and 800 K, which indicates the presence of acid sites with different strength. The relative contribution of each individual desorption peak was obtained by decomposition of the TPD profiles and integration of the desorption curves obtained, considering

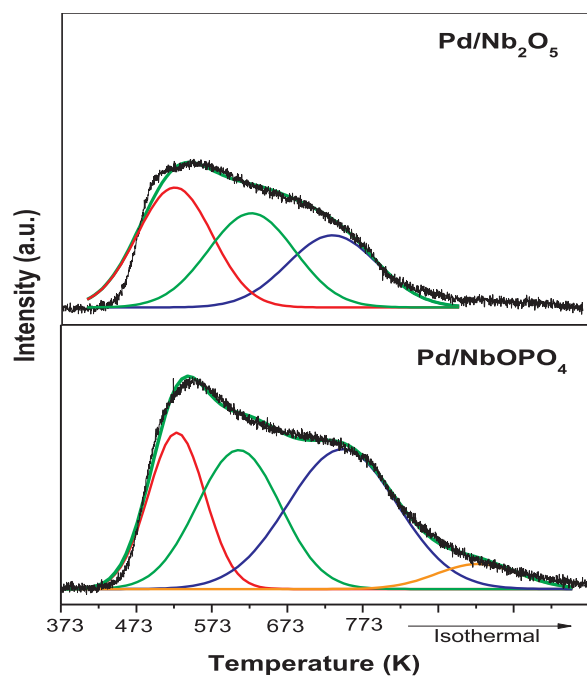


**Fig. 2.** NH<sub>3</sub>-TPD profiles for Pd/Nb<sub>2</sub>O<sub>5</sub> and Pd/NbOPO<sub>4</sub> catalysts.

**Table 1**

Total amount of NH<sub>3</sub> desorbed and acid sites strength distribution of the catalysts reduced at 573 K.

Catalyst	Ammonia desorbed (μmol/g <sub>cat</sub> )	Ammonia desorbed (μmol/m <sup>2</sup> )	Acid sites distribution (%)		
			Weak	Medium	Strong
Pd/Nb <sub>2</sub> O <sub>5</sub>	249	1.12	38	34	27
Pd/NbOPO <sub>4</sub>	383	1.24	23	31	46

the adsorption on three acid sites with different strength (weak, medium and strong). A multiple-Gaussian function was selected for fitting the experimental data. The density of acid sites as well as the distribution of the acid sites are listed in Table 1. Pd supported over NbOPO<sub>4</sub> exhibited the highest density of acid sites and a higher fraction of strong acid sites. The values of the amount of acid sites obtained in our work for niobia-supported catalysts agree very well with the data reported in the literature [34].

Figs. 3–5 show the in situ XRD patterns recorded during treatment of Pd/SiO<sub>2</sub>, Pd/Nb<sub>2</sub>O<sub>5</sub> and Pd/NbOPO<sub>4</sub> samples under different gases (He or H<sub>2</sub>) from 298 to 573 K. The diffractogram of Pd/SiO<sub>2</sub> sample at room temperature under He exhibits a line at  $2\theta = 22.48^\circ$  that is attributed to PdO phase (PDF 41-1107). When this sample is exposed to pure H<sub>2</sub> at 298 K, it is noticed that the intensity of the line corresponding to PdO decreases, whereas a new line appears at  $2\theta = 25.64^\circ$  that is likely due to the formation of Pd hydride phase [35]. Therefore, PdO is reduced to metallic Pd at room temperature, followed by the absorption of hydrogen into palladium, resulting in the formation of hydride phase. The diffractogram remained unchanged when the temperature was increased to 408 K. Further increase in the temperature to 433 K shifted this line to  $2\theta = 26.46^\circ$ , indicating the conversion of Pd hydride into metallic Pd. Hydrogen solubility in Pd decreases at high temperature and thus, heating the sample above 350 K led to the destruction of Pd hydride phase. This result has been reported in the literature during TPR experiments [36,37]. The TPR profile of Pd/SiO<sub>2</sub> and Pd/Nb<sub>2</sub>O<sub>5</sub> catalysts showed a hydrogen desorption peak at around 345 K, which was attributed to the decomposition of Pd hydride phase [37]. Therefore, this lattice expansion observed in the XRD patterns is likely due to the hydride formation.

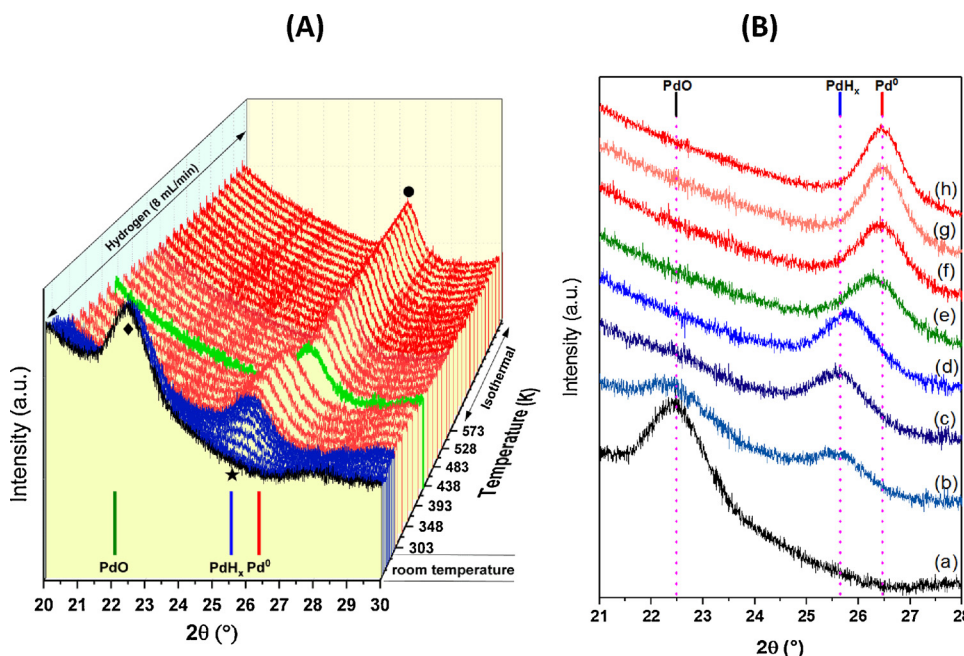


**Fig. 3.** (A) Diffractograms of Pd/SiO<sub>2</sub> obtained during reduction at different temperatures. (B) XRD patterns at selected reduction temperatures: (a) He, 298 K, (b) H<sub>2</sub> 298 K after 15 min, (c) H<sub>2</sub> 298 K after 30 min, (d) H<sub>2</sub> 408 K, (e) H<sub>2</sub> 433 K, (f) H<sub>2</sub> 458 K, (g) H<sub>2</sub> 573 K, and (h) H<sub>2</sub> 573 K after 1 h. (◆) PdO; (★) PdH; (●) Pd<sup>0</sup>.

For Pd/Nb<sub>2</sub>O<sub>5</sub> and Pd/NbOPO<sub>4</sub>, the diffractograms were similar to the silica supported catalyst. At room temperature, PdO is reduced under pure H<sub>2</sub> producing a Pd hydride phase, which is decomposed as the sample is heated above 458 K (Pd/Nb<sub>2</sub>O<sub>5</sub>) and 356 K (Pd/NbOPO<sub>4</sub>).

**Table 2** lists the average crystallite size of Pd<sup>0</sup> obtained from the diffractograms after reduction of Pd-based catalysts at 573 K for 1 h. Pd/SiO<sub>2</sub> and Pd/Nb<sub>2</sub>O<sub>5</sub> catalysts have Pd<sup>0</sup> crystallite size of 6.5 and 4.5 nm, respectively, whereas Pd/NbOPO<sub>4</sub> exhibited the largest crystallite size (9.3 nm). Pd dispersions were 15 and 22 nm for Pd/SiO<sub>2</sub> and Pd/Nb<sub>2</sub>O<sub>5</sub> catalysts, respectively [14,38].

### 3.2. HDO of model molecules

The reaction rate and product distribution for HDO of different model molecules (phenol, m-cresol, anisole and guaiacol) at 573 K and at low levels of conversion are reported in **Table 3** (Pd/SiO<sub>2</sub>), **Table 4** (Pd/Nb<sub>2</sub>O<sub>5</sub>) and **Table 5** (Pd/NbOPO<sub>4</sub>) and in supplementary information (Tables S1-S3).

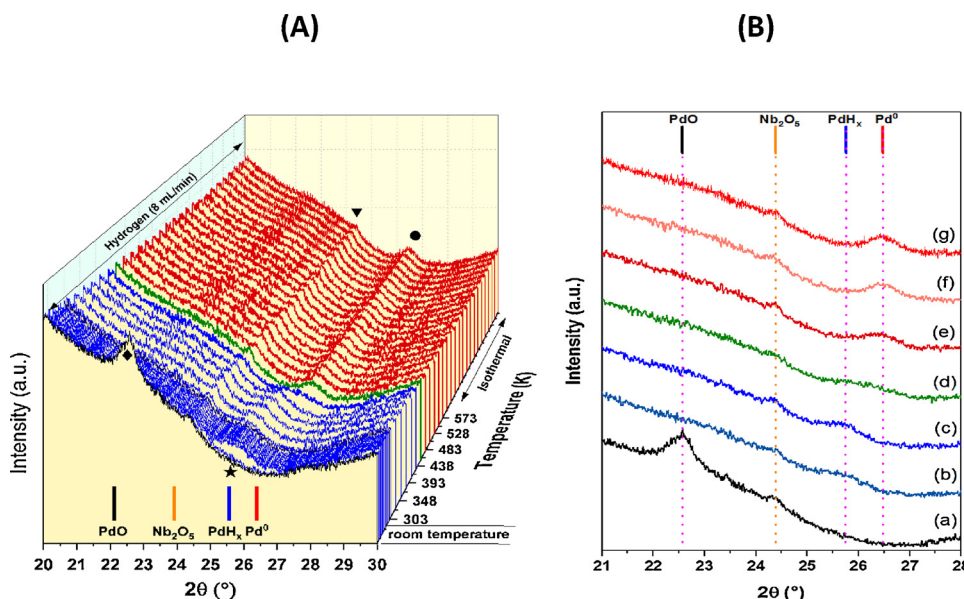


**Fig. 4.** (A) Diffractograms of Pd/Nb<sub>2</sub>O<sub>5</sub> obtained during reduction at different temperatures. (B) XRD patterns at selected reduction temperatures: (a) He 298 K, (b) H<sub>2</sub> 298 K, (c) H<sub>2</sub> 383 K, (d) H<sub>2</sub> 433 K, (e) H<sub>2</sub> 458 K, (f) H<sub>2</sub> 573 K, and (g) H<sub>2</sub> 573 K after 1 h. (◆) PdO; (★) PdH; (●) Pd<sup>0</sup>.

Pd/Nb<sub>2</sub>O<sub>5</sub> exhibited the highest reaction rate for HDO of phenol, which was 99-fold higher than that on Pd/SiO<sub>2</sub>. In addition, the supports did not show any activity under the reaction conditions used. Concerning product distribution, benzene, cyclohexanone, cyclohexanol and cyclohexane were the main products formed for all catalysts. Small amounts of biphenyl were also detected for Pd/NbOPO<sub>4</sub>. This C<sub>12</sub> hydrocarbon might be produced by the alkylation of phenolic rings with cyclohexanone over acid sites [39]. Therefore, the formation of biphenyl only on Pd/NbOPO<sub>4</sub> catalyst is likely due to its higher density of acid sites as well as the presence of Bronsted acid sites. However, product distribution depended on the type of the support. Benzene was the dominant product for niobia supported catalysts, whereas cyclohexanone was the main compound formed on Pd/SiO<sub>2</sub>. For instance, the selectivity to benzene over niobia supported catalysts was around 40-fold higher than that obtained on Pd/SiO<sub>2</sub>. Therefore, not only the activity but also the selectivity to deoxygenation strongly depends on the type of the support.

Product distribution obtained in this work agrees very well with the

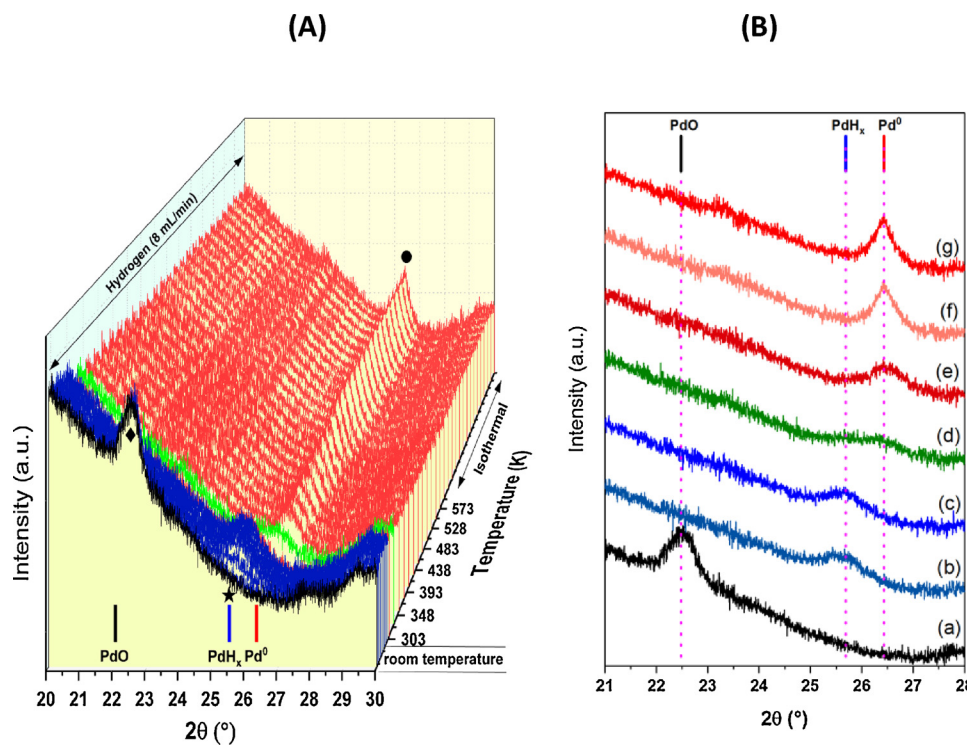


Fig. 5. (A) Diffractograms of Pd/NbOPO<sub>4</sub> obtained during reduction at different temperatures. (B) XRD patterns at selected reduction temperatures: (a) He 298 K, (b) H<sub>2</sub> 298 K, (c) H<sub>2</sub> 308 K, (d) H<sub>2</sub> 333 K, (e) H<sub>2</sub> 358 K, (f) H<sub>2</sub> 573 K, and (g) H<sub>2</sub> 573 K after 1 h. (◆) PdO; (★) PdH<sub>x</sub>; (●) Pd<sup>0</sup>.

Table 2  
Crystallite size of Pd<sup>0</sup> and Pd dispersion of the catalysts reduced at 573 K.

Catalyst	d <sub>Pd</sub> (nm) <sup>a</sup>	D <sup>b</sup> (%)
Pd/SiO <sub>2</sub>	6.5	15
Pd/Nb <sub>2</sub> O <sub>5</sub>	4.5	22
Pd/NbOPO <sub>4</sub>	9.3	11

<sup>a</sup> Particle size of Pd<sup>0</sup> calculated by Scherrer equation.

<sup>b</sup> Pd dispersion calculated by XRD for catalyst reduced at 573 K.

reaction mechanism recently proposed by our group that is based on the tautomerization of phenol [12–14,38]. The hydrogenation of the ring leading to the formation of cyclohexanone and cyclohexanol was the main reaction pathway over Pd supported on SiO<sub>2</sub>, Al<sub>2</sub>O<sub>3</sub>, CeO<sub>2</sub> and

CeZrO<sub>2</sub> catalysts. The carbonyl group is preferentially hydrogenated to 2,4-cyclohexadienol, producing benzene by dehydration over ZrO<sub>2</sub>, TiO<sub>2</sub> and Nb<sub>2</sub>O<sub>5</sub> supported catalysts. This is due to the strong interaction between the oxygen of the intermediate molecule formed and the oxophilic sites represented by Zr<sup>4+</sup>/Zr<sup>3+</sup>, Ti<sup>4+</sup>/Ti<sup>3+</sup> and Nb<sup>4+</sup>/Nb<sup>5+</sup> cations near the perimeter of the metal particles.

The results obtained for HDO of m-cresol were quite similar to those ones obtained for phenol. Pd/Nb<sub>2</sub>O<sub>5</sub> was the most active catalyst, showing a reaction rate that is 125-fold higher than that for Pd/SiO<sub>2</sub>. The main products formed were toluene, methyl-cyclohexanone, methyl-cyclohexanol for all catalysts. A small amount of 1-methyl-4-(4-methylphenyl)benzene was also produced over Pd/NbOPO<sub>4</sub>, which could also be attributed to the acid sites of this catalyst. The similarity between the results for HDO of m-cresol and phenol suggests the same reaction mechanism for both molecules. This result is due to the fact

Table 3  
Products distribution for hydrodeoxygenation of different model molecules over Pd/SiO<sub>2</sub> catalyst (T<sub>reaction</sub> = 573 K, 1 atm).

Substrate	X (%)	Rate of HDO (mmol·min <sup>-1</sup> ·g <sub>cat</sub> <sup>-1</sup> )	Selectivity (%)					
	15.8	0.01						
			2.1	91.6	6.3			
	4.5	0.007						
			8.3	80.2	11.5			
	5.1	0.04						
			29.4	31.4	4.5	0.9	1.7	22.7 9.4
	14.5	0.00						
			41.8	4.7	0.8			8.0 44.1

**Table 4**Products distribution for hydrodeoxygenation of different model molecules over Pd/Nb<sub>2</sub>O<sub>5</sub> catalyst (T<sub>reaction</sub> = 573 K, 1 atm).

Substrate	X (%)	Rate of HDO (mmol·min <sup>-1</sup> ·g <sub>cat</sub> <sup>-1</sup> )	Selectivity (%)							
	9.3	0.99		85.2		13.6	1.2			
	8.7	0.88		94.1		3.8	2.1			
	7.8	0.26		45.0		6.3		0.9	CH <sub>4</sub> 9.7	CH <sub>3</sub> OH 36.7
	11.0	0.057		13.4		30.0		2.1	CH <sub>4</sub> 8.0	CH <sub>3</sub> OH 36.0

that both molecules exhibits the same adsorption mode with the formation of phenoxy species through the dissociative adsorption of the phenolic compound over the metal oxide cation (Lewis acid site) [12–14]. Therefore, the methyl group of the aromatic ring does not affect the reaction pathways since it is not involved in the adsorption of the molecule. These results are in agreement with the reaction mechanism proposed for these molecules in the literature [8–10,12,14] and it could be summarized in **Scheme 1**.

For HDO of anisole, Pd/SiO<sub>2</sub> and Pd/NbOPO<sub>4</sub> catalysts had approximately the same reaction rate, whereas Pd/Nb<sub>2</sub>O<sub>5</sub> exhibited the highest activity among the catalysts. For all catalysts, the main products observed were benzene, phenol, methane and methanol along with very small amounts of cyclohexane, cyclohexanone, cyclohexanol and methoxycyclohexane. It is important to stress that SiO<sub>2</sub> and Nb<sub>2</sub>O<sub>5</sub> supports were not active for HDO of anisole but NbOPO<sub>4</sub> has a significant activity (0.016 mmol/(g<sub>cat</sub>·min)) in comparison to the catalyst, producing only phenol.

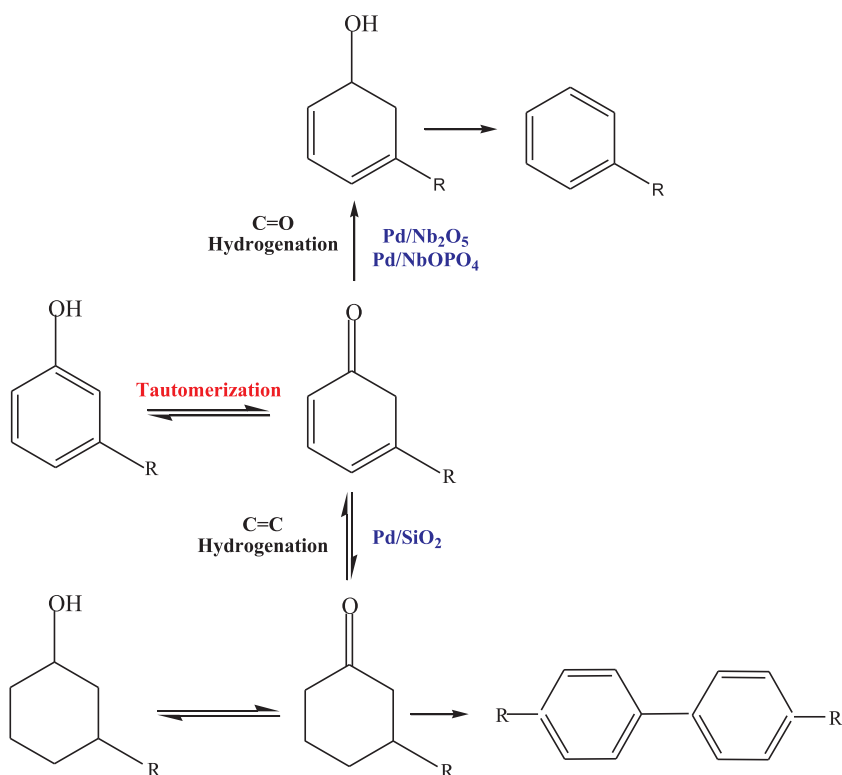
As observed for HDO of phenol and m-cresol, the products distribution was affected by the type of the support. Benzene and methanol were mainly formed over the Pd/Nb<sub>2</sub>O<sub>5</sub> catalyst, whereas significant production of phenol and methane occurred on Pd/SiO<sub>2</sub>. Methane can be generated from the methoxy group of the anisole molecule and/or the hydrogenolysis of the aromatic ring. However, no hydrogenolysis

has been observed in the hydrodeoxygenation of phenolics under the same reaction conditions on Pd catalysts [9,12,40]. In fact, the phenol and methane yields were similar, indicating that the cleavage of the C–O bond from the methoxy group is favored over Pd/SiO<sub>2</sub>. The formation of benzene and methanol suggests that the demethoxylation of anisole molecule takes place, which is in agreement with the benzene and methanol yields that are very close on Pd/Nb<sub>2</sub>O<sub>5</sub>. This is the main reaction pathway on Pd/Nb<sub>2</sub>O<sub>5</sub> catalyst. The slightly higher benzene yield indicates that benzene may also be produced by the tautomerization of phenol formed. **Scheme 2** shows the reaction pathways for HDO of anisole on the catalysts of our work. The molecule marked in red indicates that this product may follow the reaction pathway previously described in **Scheme 1**. However, Pd/NbOPO<sub>4</sub> exhibited a higher selectivity to phenol than Pd/Nb<sub>2</sub>O<sub>5</sub>. In this case, the comparatively high selectivity to phenol may be due to reaction over the NbOPO<sub>4</sub> support, which was determined to be active in the absence of Pd under reaction conditions explored here.

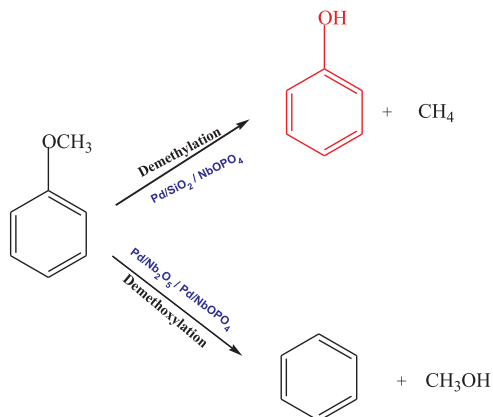
Tan et al. [41] conducted a combined experimental and theoretical study of the hydrodeoxygenation of anisole over Pt, Ru and Fe supported on silica catalysts. The catalysts were tested in the vapor phase reaction at 648 K and atmospheric pressure. In parallel, density functional theory (DFT) calculations were employed to the metals surfaces to understand the possible reaction mechanism. They proposed that the

**Table 5**Products distribution for hydrodeoxygenation of different model molecules over Pd/NbOPO<sub>4</sub> catalyst (T<sub>reaction</sub> = 573 K, 1 atm).

Substrate	X (%)	Rate of HDO (mmol·min <sup>-1</sup> ·g <sub>cat</sub> <sup>-1</sup> )	Selectivity (%)						
	8.4	0.03		83.3		5.8		5.6	
	13.0	0.07		90.0		4.1		5.2	
	6.1	0.02		21.7		36.3		0.4 	1.2 CH <sub>4</sub> 17.7 CH <sub>3</sub> OH 19.7
	17.0	0.005		2.5		44.0		5.2 CH <sub>4</sub> 4.9 CH <sub>3</sub> OH 39.1	



**Scheme 1.** Reaction routes for HDO of substituted phenolic compounds over supported Pd catalysts (R = H; CH<sub>3</sub>).



**Scheme 2.** Reaction routes for HDO of anisole over supported Pd catalysts. The molecule marked in color indicates that this product may follow the reaction pathway previously described in **Scheme 1**.

sequential dehydrogenation at the –CH<sub>3</sub> side group is more favorable than C–O bond breaking. Then, the surface phenoxy can undergo hydrogenation to form phenol or to break the C<sub>aryl</sub>–O bond to form phenyl and benzene by hydrogenation. In that work, the Pt/SiO<sub>2</sub> catalyst favored the hydrogenation of the phenoxy species to form phenol as a primary product and the Ru/SiO<sub>2</sub> and Fe/SiO<sub>2</sub> catalysts favored the breaking of C–O bond to form benzene.

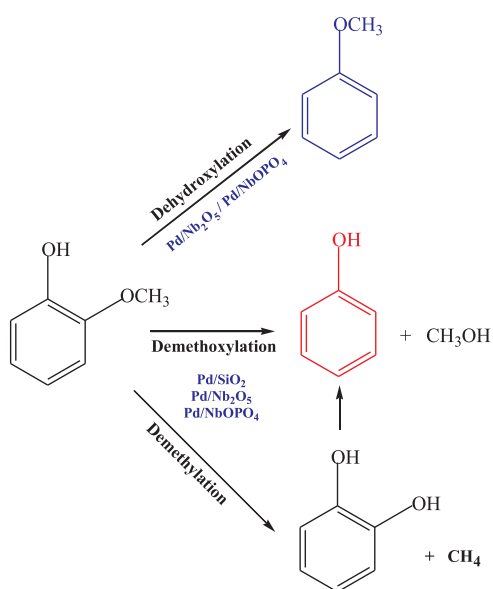
In the present work, a similar mechanism observed by Tan et al. [41] for Pt/SiO<sub>2</sub> catalyst can be proposed for the Pd/SiO<sub>2</sub> catalyst. In this case, phenol is formed by the cleavage of the C<sub>alkyl</sub>–O bond from the methoxy group, which can further react to form cyclohexanone and cyclohexanol. On the other hand, for Pd/Nb<sub>2</sub>O<sub>5</sub> catalyst, the high selectivity to methanol and benzene indicates that the direct C<sub>aryl</sub>–O cleavage occurs as it was observed for Ru/SiO<sub>2</sub> and Fe/SiO<sub>2</sub> catalysts. According to the literature, Ru and Fe are more oxophilic metals, which favors the direct hydrodeoxygenation of phenolic compounds

[8,9,20,40,42].

The comparatively high rates of demethoxylation observed over Pd/Nb<sub>2</sub>O<sub>5</sub> are consistent with a previous report from our group in which the strong interaction between the oxophilic sites represented by Nb<sup>5+</sup>/Nb<sup>4+</sup> cations and the oxygen from the phenol molecule results in a high selectivity to deoxygenated products [38]. For Pd/NbOPO<sub>4</sub> catalyst, the high selectivity to phenol is attributed to the acid sites of the support that promotes the scission of the C–O bond of the methoxy group. This result was reported by Zhu et al. [43], who studied the HDO of anisole over HBeta zeolite. The main products formed were phenol and methylanisole, indicating that the demethylation of anisole is the primary reaction. The authors proposed that the methoxy group was decomposed on the acid site, followed by the alkylation of another anisole molecule by the methyl group formed. In our work, the absence of methylanisole compounds suggests that the acidity is not enough to promote alkylation and then, carbon deposits accumulate on catalyst surface.

The HDO of guaiacol reaction over Pd/SiO<sub>2</sub> catalyst produced mainly phenol and methanol, indicating that demethoxylation is the main reaction pathway. Small amounts of methane and cyclohexanone were also formed, but catechol was not observed. The removal of methane from the methoxy group could produce catechol, which was likely converted to phenol and then cyclohexanone. For Pd/Nb<sub>2</sub>O<sub>5</sub> catalyst, the main products formed were also phenol and methanol but in contrast to Pd/SiO<sub>2</sub>, significant amounts of benzene, anisole and methane were also observed. The production of benzene over Pd/Nb<sub>2</sub>O<sub>5</sub> is attributed to the conversion of phenol formed to benzene via the tautomerization route, as previously described in **Scheme 1**. In addition, anisole was also produced, suggesting that the dehydroxylation of guaiacol may follow the same reaction pathway proposed for phenol. The formation of methane indicates that catechol may also be formed but is rapidly dehydrated to phenol and consequently not observed as a reaction product or it may remain adsorbed on the surface.

For Pd/NbOPO<sub>4</sub> catalyst, the major products were also phenol and methanol. Small amounts of benzene, anisole and veratrole were also



**Scheme 3.** Reaction routes for HDO of guaiacol over supported Pd catalysts. The molecule marked in color indicates that this product may follow the reaction pathway previously described in *Schemes 1* (phenol) and *2* (anisole).

detected. The formation of veratrole may occurs through the alkylation of the anisole by methanol over the acid sites. *Scheme 3* shows the main reaction routes for HDO of guaiacol over supported Pd catalysts. The molecule marked in color indicates that this product may follow the reaction pathway previously described in *Schemes 1* (phenol) and *2* (anisole).

### 3.3. General reaction mechanism

HDO of different model molecules representative of different fractions of lignocellulosic biomass has been extensively studied to design catalysts for the bio-oil upgrading. Phenolic compounds have been used to represent lignin-derived products and these studies includes mainly phenol [12–19], cresol [8–11], anisole [21–23], guaiacol [24–26]. These model molecules contain different functional groups ( $-\text{OH}$  and  $-\text{OCH}_3$ ) on the aromatic ring. Therefore, catalysts for the HDO of these model molecules should be able to remove these  $-\text{OH}$  and  $-\text{OCH}_3$  functional groups, which involves the cleavage of different types of C–O bond: the aromatic  $\text{C}_{\text{aryl}}-\text{O}$  bond and the aliphatic  $\text{C}_{\text{alkyl}}-\text{O}$  bond. Consequently, different mechanisms have been proposed in the literature. In spite of a large number of works investigating the mechanism for HDO of different phenolic compounds, there are only a few studies comparing the performance of the same catalysts on several HDO reactions.

In our work, the HDO of phenol, m-cresol, anisole and guaiacol was carried out over  $\text{Pd/SiO}_2$ ,  $\text{Pd/Nb}_2\text{O}_5$ , and  $\text{Pd/NbOPO}_4$  catalysts to study the effect of the support on the deoxygenation activity for the different molecules. Phenol, m-cresol and anisole are interesting molecules because they have only one functional group attached to the aromatic ring ( $-\text{OH}$  or  $-\text{OCH}_3$ ), whereas guaiacol contains both functional groups. Therefore, the study of the HDO mechanism for the removal of each functional group could provide important information for the understanding of the mechanism for HDO of guaiacol.

$\text{Pd/Nb}_2\text{O}_5$  exhibited the highest deoxygenation activity for all molecules among the catalysts. This is likely due to the smaller Pd particle size of this catalyst calculated by *in situ* XRD experiments. The HDO reaction takes place at the metal-support interface and then, smaller particle size leads to a higher metal-support contact, improving catalyst activity [14].

For instance, the HDO of phenol or m-cresol over  $\text{Pd/SiO}_2$  produced

mainly hydrogenation products (cyclohexanone, cyclohexanol, methylcyclohexanone, methylcyclohexanol). These results agree very well with the tautomerization mechanism proposed in the literature [9,12,38,40]. For the HDO of anisole over this catalyst, phenol and methane were the main products formed, indicating that the cleavage of the  $\text{C}_{\text{alkyl}}-\text{O}$  bond from the methoxy group is favoured over  $\text{Pd/SiO}_2$ . Benzene and methanol were also produced via demethoxylation. DFT calculations demonstrated that the first step for HDO of anisole involves the dehydrogenation of  $\text{CH}_3$  group, which facilitates the  $\text{C}_{\text{alkyl}}-\text{O}$  bond breaking [44]. However, the HDO of guaiacol reaction over  $\text{Pd/SiO}_2$  catalyst produced mainly phenol and methanol, indicating that demethoxylation is more favourable than demethylation. In addition, benzene and catechol were not detected. Therefore, the presence of the hydroxyl group on the guaiacol molecule changes completely the main reaction pathway observed on  $\text{Pd/SiO}_2$  catalyst. The presence of the  $-\text{OH}$  group attached on the aromatic ring favoured the cleavage of  $\text{C}_{\text{aryl}}-\text{O}$  bond.

The type of support significantly affected product distribution for all reactions.  $\text{Pd/Nb}_2\text{O}_5$  catalyst exhibited a high selectivity to deoxygenated products for HDO of phenol or m-cresol (benzene and toluene). This result is attributed to the strong interaction between the oxygen of the intermediate molecule formed and the oxophilic sites represented by  $\text{Nb}^{4+}/\text{Nb}^{5+}$  cations near the perimeter of the metal particles [38]. For HDO of anisole, the niobia support promoted the demethoxylation (benzene) rather than demethylation (phenol). According to the literature [41], the HDO of anisole over more oxophilic metals such as Fe involves firstly the dehydrogenation of the methyl group, which facilitates the cleavage of the  $\text{C}_{\text{alkyl}}-\text{O}$  bond with the formation of the surface phenoxy species. The oxophilic metal promotes the cleavage of the  $\text{C}_{\text{aryl}}-\text{O}$  bond of the phenoxy species to form benzene instead of its hydrogenation to form phenol. The result obtained for HDO of anisole over  $\text{Pd/Nb}_2\text{O}_5$  catalyst agrees with this proposal. However, the HDO of guaiacol produced mainly phenol and methanol, with only small amounts of benzene. Since benzene was the main product obtained for the HDO of phenol or anisole, this result shows that the presence of both functional groups strongly affects the deoxygenation activity of the  $\text{Pd/Nb}_2\text{O}_5$  catalyst. This is likely due to the adsorption mode of guaiacol molecule over the catalyst surface. In this case, the guaiacol molecule adsorbs through the oxygen atom of methoxy group and follows the reaction pathways proposed for anisole molecule over an oxophilic site (Fe or niobia). The removal of the methoxy group leads to the formation of phenol that rapidly desorbs before further reaction.

### 3.4. Stability of $\text{Pd/Nb}_2\text{O}_5$ catalyst for HDO of phenol and guaiacol

Considering the highest deoxygenation activity of the  $\text{Pd/Nb}_2\text{O}_5$  catalyst for the HDO reaction of different model molecules studied (phenol, m-cresol, anisole and guaiacol), long-term tests were performed to investigate the stability of this catalyst. Therefore, the HDO of phenol and guaiacol were carried out for 22 h and the results obtained are shown in *Fig. 6*.

The conversion significantly decreases as a function of the reaction time, regardless of the model molecule. For the reaction with phenol, the yields of benzene, cyclohexane and biphenyl also decrease, following the same trend observed for the phenol conversion. However, for the reaction with guaiacol, the products distribution changes as a function of TOS. The yield of benzene decreases significantly, whereas the yields of phenol and anisole increases achieving a maximum at around  $\sim 200$  min of reaction and then, they decrease continuously with TOS. Methanol yield decreases and levels off at 50 min of TOS, remaining constant up to 300 min. Then, it begins to decrease again.

According to the results for the HDO of the different model molecules investigated at low conversion, phenol reacts producing mainly benzene over  $\text{Pd/Nb}_2\text{O}_5$  catalyst. The demethoxylation of guaiacol producing phenol and methanol is the main route observed for this

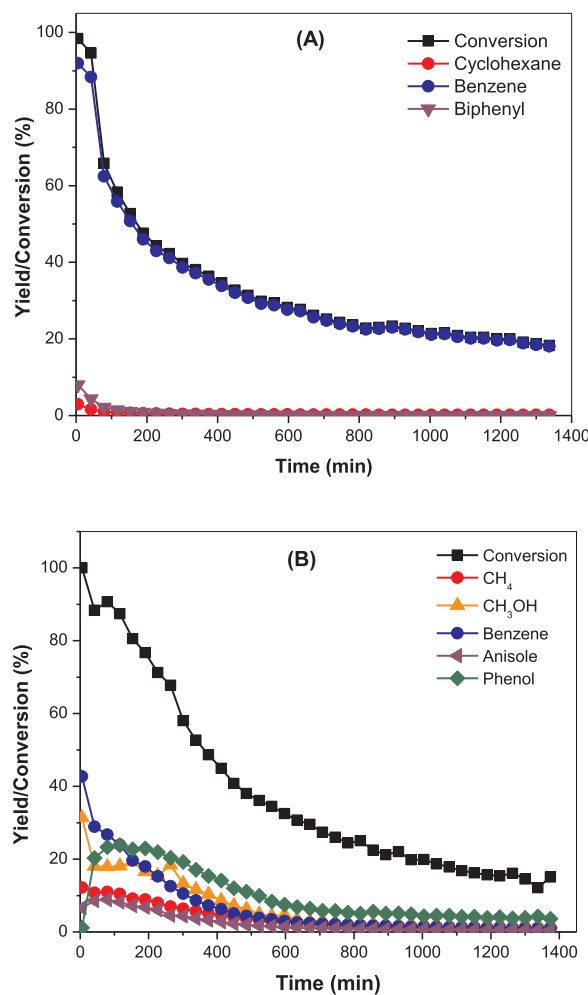


Fig. 6. Conversion and yield of the products as a function of TOS for Pd/Nb<sub>2</sub>O<sub>5</sub> catalysts in (A) phenol and (B) guaiacol HDO reaction.

catalyst. This result suggests that at high conversion benzene is formed by deoxygenation of the phenol mainly produced via demethoxylation of guaiacol. The decrease in the conversion of guaiacol is accompanied by a decrease in the yield of benzene whereas the formation of phenol increases steadily and methanol yield remains constant up to 300 min. These results suggest that the active sites responsible for the conversion of phenol into benzene are being deactivated. After ~300 min, the phenol and methanol yields decrease simultaneously, indicating that the sites involved on the demethoxylation are also affected.

In order to further investigate the mechanism of catalyst deactivation, the used catalysts after the stability tests were characterized by temperature programmed oxidation and cyclohexane dehydrogenation to get insights into the possible formation of carbon deposits or metallic sintering.

The dehydrogenation of cyclohexane reaction was carried out after the HDO of phenol and guaiacol reactions without exposure of the catalyst to air to determine the changes in Pd dispersion during reaction. The ratio between the reaction rates of dehydrogenation of cyclohexane at 543 K over fresh and used (after 22 h of HDO of phenol and guaiacol reactions) catalysts were 17 and 7 after phenol and guaiacol reactions respectively, indicating a significant decrease in the Pd dispersion during both reactions.

Taking into account that the HDO reaction requires a bifunctional catalyst, the loss of the metal particle-support interface might contribute to the drastic catalyst deactivation observed during the reactions. The decrease of this interface may be caused by Pd sintering or coverage of Pd particles by carbonaceous deposits.

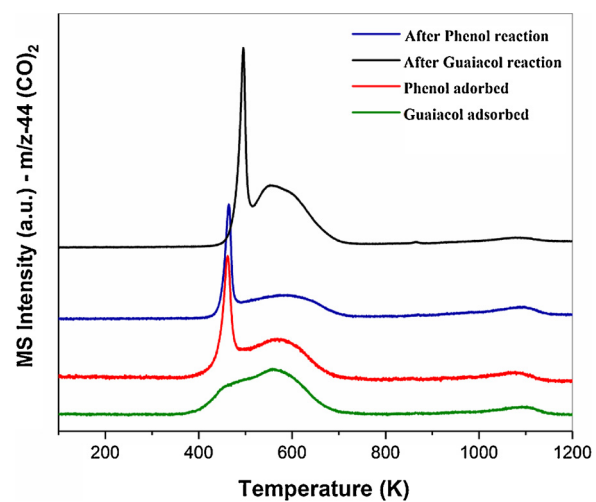
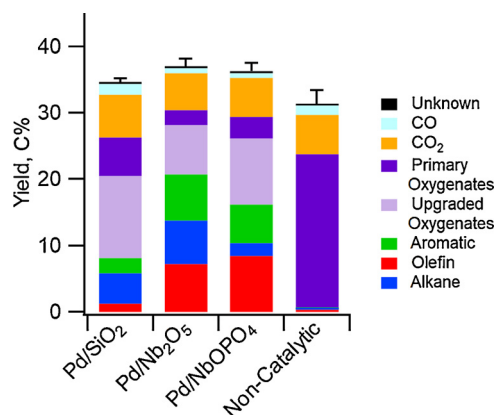


Fig. 7. TPO profiles of the spent catalysts after HDO reaction of phenol and guaiacol at 573 K for 22 h.

Temperature programmed oxidation (TPO) was used to investigate the formation of carbonaceous species on the used catalysts after 22 h of TOS. The TPO profiles (Fig. 7) of the spent catalysts after HDO of phenol and guaiacol exhibited one narrow peak at 473–500 K and a broad peak between 523 and 673 K. For the HDO of phenol, the intensity of the second peak is very weak. These two different oxidation regions can either be due to the presence of two different types of carbons or to a different location of the carbon on the surface of the catalyst [45]. However, the first peak is located at low temperature and it is unlikely that this corresponds to the oxidation of carbon deposits. Recently, Gao et al. [46] attributed the deactivation of different catalysts supported on carbon, tested on HDO of guaiacol, to the presence of aromatic compounds such as naphthalene and biphenyl adsorbed on the surface of the catalysts.

To investigate the role of adsorbed species on the deactivation of Pd/Nb<sub>2</sub>O<sub>5</sub> catalyst, phenol or guaiacol were adsorbed and then, TPO analyses were carried out. The TPO profile obtained after adsorption of phenol was quite similar to that of the used catalyst after HDO of phenol. This result indicates that the peaks observed could be assigned the oxidation of phenol adsorbed on the catalyst surface. The TPO profiles of the spent catalyst after HDO of guaiacol and of the adsorbed guaiacol were very close, except for the intensity of the first peak that was more intense after reaction.

De Souza et al. [14] investigated the deactivation of Pd supported on different oxides for HDO of phenol during 20 h of TOS. The authors observed a strong deactivation for Pd/SiO<sub>2</sub>, Pd/Al<sub>2</sub>O<sub>3</sub>, Pd/ZrO<sub>2</sub> and Pd/TiO<sub>2</sub> catalysts. Raman spectroscopy of the used catalysts was performed and the presence of carbon residues on the catalyst surface was not detected. They proposed that the Pd sintering and the blocking of the acid sites on the support are the main causes for the catalyst deactivation. To monitor the evolution of the surface species formed on the catalysts for the HDO reaction, DRIFTS spectra were recorded during 6 h of reaction under a steady flow of phenol/H<sub>2</sub> mixture at same reaction temperature (573 K). DRIFTS experiments under reaction conditions revealed a buildup of phenoxy and intermediate species during reaction. These species remained adsorbed on the Lewis acid sites, blocking those sites and inhibiting further reactant adsorption. The growth of Pd particle size decreases the metal-support interface where the HDO of phenol reaction takes place and then, catalyst deactivates. However, the adsorption strength of the model molecule with the oxides could also lead to catalyst deactivation. De Souza et al. [14] and Barrios et al. [38] measured the strength of the interaction between the oxygen of the model molecule and the metal cations of different supports (CeO<sub>2</sub>, CeZrO<sub>2</sub>, Al<sub>2</sub>O<sub>3</sub>, SiO<sub>2</sub>, ZrO<sub>2</sub>, TiO<sub>2</sub>, Nb<sub>2</sub>O<sub>5</sub>) by DRIFTS



**Fig. 8.** The yield of various product classes observed during the deoxygenation of pine pyrolysis vapors at 673 K and 0.05 MPa H<sub>2</sub>. Pyrolysis was performed in a separate upstream reactor at 773 K. Error bars are based on the total yield and represent  $\pm \sigma/2$ .

experiments of adsorbed cyclohexanone. The stronger interaction between the oxygen from the carbonyl group and oxophylic cation was observed for the niobia support. Therefore, the strong adsorption of phenol or guaiacol on the oxophylic sites represented by Nb<sup>4+</sup>/Nb<sup>5+</sup> cations present on the support may contribute to deactivation of the catalyst due to the accumulation of oxygenated intermediates that remain adsorbed on the active sites and inhibits further reaction. Furthermore, the two different regions observed in the TPO profiles could be attributed to oxidation of oxygenated molecules with different degrees of strength adsorption: less strongly adsorbed molecules are oxidized at lower temperatures whereas the more strongly adsorbed ones are oxidized at higher temperatures.

### 3.5. HDO of pine pyrolysis vapors

Experiments were conducted using a tandem py-GCMS/FID system to assess the performance of Pd/SiO<sub>2</sub>, Pd/Nb<sub>2</sub>O<sub>5</sub>, and Pd/NbOPO<sub>4</sub> for the HDO of pine pyrolysis vapors. The carbon yields observed for each catalyst are provided in the supplementary information (Tables S4–S6) and summarized in Fig. 8. The overall carbon yield during catalytic upgrading varied from 34.2% over Pd/SiO<sub>2</sub> to 36.9% over Pd/Nb<sub>2</sub>O<sub>5</sub>. In all cases, these values are elevated compared to the 31.2% yield observed in the absence of a catalyst. The comparatively high yields observed during catalytic upgrading are attributed at the cracking of high molecular weight, non-chromatographable oligomers into smaller fuel range products. The overall carbon yields observed during pine pyrolysis in this work are in good agreement with previously reported values for lignin pyrolysis ( $\approx 35\%$ ) using a similar reactor system and conditions [5]. However, they are lower than values reported from pyrolysis of corn stover ( $\approx 45\%$ ) [5]. A comparison between the non-catalytic experiments indicates that an increase in the production of CO and CO<sub>2</sub> is primarily responsible for the higher corn stover yields. These light gasses can be formed from decarbonylation and/or decarboxylation of acids, which are produced in higher concentrations during pyrolysis of corn stover compared to pine [44]. The variation in lignin structure between woody vs herbaceous biomass may also impact pyrolysis yields [47]. For example, Zhou et al. demonstrated that the yield of liquid products was 7.4–10.1% lower during fast pyrolysis of lignin derived from loblolly pine compared to lignin derived from corn stover [48]. The overall yields reported here are higher than previously observed during the upgrading of pine pyrolysis vapors using ZSM-5 catalysts operated at 773 K in the absence of hydrogen (11–17%) [4]. This improvement highlights the potential benefits of HDO, in which hydrogen is utilized to minimize the production of carbon-containing light gasses and reduce coking.

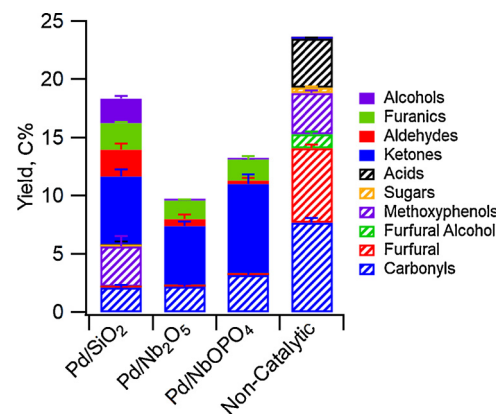


**Fig. 9.** The carbon yield of oxygenated products observed during the hydrodeoxygenation of pine pyrolysis vapors at 673 K and 0.05 MPa H<sub>2</sub>. Pyrolysis was performed in a separate upstream reactor at 773 K. Patterned markers indicated unreacted primary oxygenates, and solid markers indicate partially upgraded oxygenates. Error bars represent  $\pm \sigma/2$ .

In Fig. 9, oxygenates are divided into primary and partially upgraded compounds. Primary oxygenates represent unreacted molecules formed during pyrolysis, whereas partially upgraded oxygenates are intermediates formed during the production of hydrocarbons. All three catalysts were effective for reducing the total yield of oxygenated products. The extent of deoxygenation was highest over the Pd/Nb<sub>2</sub>O<sub>5</sub> and Pd/NbOPO<sub>4</sub> catalysts, which effectively reduced the yield of oxygenates by 59% and 43% on a relative basis, respectively. Comparatively, Pd/SiO<sub>2</sub> decreased the yield of oxygenates by 24% on a relative basis and exhibited the largest fraction of unreacted primary compounds. The effectiveness of Pd/Nb<sub>2</sub>O<sub>5</sub> and Pd/NbOPO<sub>4</sub> for deoxygenation is in good agreement with the model compound results described above and is attributed to oxophilic Nb cationic sites on the support, which have been previously reported to promote C–O bond scissions by forming strong interactions with oxygenated reactants [38].

Despite the reduction in oxygenate yield, some partially oxygenated products were observed over each catalyst. The production of oxygenates in this work contrasts with previous results in which complete deoxygenation to form linear alkanes and aromatics was reported during the catalytic upgrading of corn stover and lignin fast pyrolysis vapors over MoO<sub>3</sub> [5]. This variation in deoxygenation may be partially explained by the difference in catalyst to biomass ratios (C:B) utilized for each pulse. The MoO<sub>3</sub> experiments were performed using 200 mg of catalyst and 0.25–0.30 mg of biomass, resulting in a C:B ratio of 666–800. The experiments reported here were performed with 10 mg of catalyst and 0.50 mg of biomass, resulting in a C:B ratio of 20. The comparatively low loading of Pd/SiO<sub>2</sub>, Pd/Nb<sub>2</sub>O<sub>5</sub>, and Pd/NbOPO<sub>4</sub> was selected to probe catalytic performance under partial deoxygenation conditions, which allows for a comparison of oxygenated product yield (Fig. 9). For the non-catalytic experiments, acids (e.g., acetic acid and propanoic acid), carbonyls (e.g., acetaldehyde and hydroxypropanone), furanics (e.g., furfural and furfuryl alcohol) and methoxyphenols (e.g., guaiacol and vanillin) were the main oxygenated products detected, which is consistent with previous reports [49–51].

In all cases, the presence of a catalyst either eliminated or significantly reduced the yield of acids, which reduces the corrosivity of the resulting pyrolysis oil. Over Pd/Nb<sub>2</sub>O<sub>5</sub> and Pd/NbOPO<sub>4</sub>, the conversion of acetic acid corresponded with an increase in the formation of acetone, suggesting that these catalysts may be effective for promoting ketonization reactions. Interestingly, Lu et al. [7] have previously reported an increase in the acid content after catalytic upgrading of poplar wood pyrolysis vapors using cerium modified Pd/TiO<sub>2</sub>. However, in the same report it was demonstrated that cerium modified Pd/ZrO<sub>2</sub>–TiO<sub>2</sub> is effective for reducing the acid concentration, further

highlighting the potential impacts of the support material on upgrading performance. In this work, the yield of carbonyl compounds during catalytic upgrading was greater than or equal to the yield observed in the absence of a catalyst. Some primary carbonyls (e.g., acetaldehyde) passed over the catalysts without reacting. However, the majority of the primary carbonyls were converted to ketones, particularly in the presence of Pd/Nb<sub>2</sub>O<sub>5</sub> or Pd/NbOPO<sub>4</sub>. The increased yield of carbonyl compounds may be related to the conversion of acids or the cracking of high molecular weight oligomers which were undetectable during the non-catalytic experiments. Increased yield of ketones and cyclopentanones was also reported during the catalytic upgrading of poplar wood pyrolysis vapors over Pd, Ru, and Ce modified TiO<sub>2</sub> and ZrO<sub>2</sub>–TiO<sub>2</sub> catalysts [7]. In addition to these products, the Pd/SiO<sub>2</sub> catalyst exhibited measurable yields of methoxyphenols, acids, and alcohols. The absence of methoxylphenols over Pd/Nb<sub>2</sub>O<sub>5</sub> and Pd/NbOPO<sub>4</sub> is consistent with an increase in the yield of deoxygenated aromatics. The effectiveness of these materials for the deoxygenation of methoxyphenols is in agreement with the model compound results, in which the reaction rate for guaiacol HDO was determined to be higher over Pd/Nb<sub>2</sub>O<sub>5</sub> than Pd/SiO<sub>2</sub>. Interesting, phenol was the dominant product during guaiacol HDO, but no phenolic products were detected during upgrading of pine pyrolysis vapors. This difference may be due to the higher temperatures utilized during the whole vapor upgrading experiments (673 vs 573 K), which could provide sufficient thermal energy to overcome the barrier for scission of the aryl–OH bond and increase selectivity to deoxygenated aromatic products.

The distribution of deoxygenated products is provided in Table S6. The dominant aromatic product over Pd/SiO<sub>2</sub> was benzene, whereas Pd/Nb<sub>2</sub>O<sub>5</sub> and Pd/NbOPO<sub>4</sub> favoured the production of alkylated one and two ring aromatics. The production of C<sub>4</sub> olefins was observed over all the catalysts. However, Pd/Nb<sub>2</sub>O<sub>5</sub> and Pd/NbOPO<sub>4</sub> also formed C<sub>5</sub>–C<sub>9</sub> olefins, which were not detected over Pd/SiO<sub>2</sub> (e.g., methylbutene and methylcyclopentene). The dominant alkane products included methane, ethane, propane, and methyl pentane. Among all the deoxygenated products, the yields of aromatics and olefins were higher than the yield of alkanes over Pd/Nb<sub>2</sub>O<sub>5</sub> and Pd/NbOPO<sub>4</sub>. Conversely, Pd/SiO<sub>2</sub> exhibited higher yields to alkanes than aromatics and olefins. The comparatively high yield of hydrogenated products may suggest that the reactivity of Pd/SiO<sub>2</sub> is driven by the metallic phase, while additional reaction pathways over the Nb-containing supports promote deoxygenation without requiring full ring hydrogenation.

#### 4. Conclusions

In this work, we have investigated the effects of varying the type of support (SiO<sub>2</sub>, Nb<sub>2</sub>O<sub>5</sub>, NbOPO<sub>4</sub>) on the HDO mechanism for the removal of different functional groups from aromatic ring: hydroxyl (phenol, m-cresol), methoxy (anisole) and hydroxyl and methoxy (guaiacol).

The type of support significantly affected the activity and the selectivity to deoxygenation, regardless of the model molecule. Pd/Nb<sub>2</sub>O<sub>5</sub> was the most active catalyst for HDO of phenol and m-cresol. Benzene and toluene were the main products formed over niobia supported catalysts, whereas hydrogenated products (cyclohexanone and methylcyclohexanone) were mainly produced on Pd/SiO<sub>2</sub>. The product distribution obtained for both molecules agrees very well with the reaction mechanism based on the tautomerization of phenol and the formation of a cyclohexadienone. The hydrogenation of the ring from this intermediate produces cyclohexanone/methylcyclohexanone and cyclohexanol/methylcyclohexanol and is the typical reaction pathway on Pd/SiO<sub>2</sub> catalyst. The hydrogenation of the carbonyl group from the ketotautomer intermediate leads to the formation of 2,4-cyclohexadienol, producing benzene by dehydration. This reaction route is favoured over niobia supported catalysts, which is due to the strong interaction between the oxygen of the intermediate molecule formed and the oxophilic sites represented by Nb<sup>4+</sup>/Nb<sup>5+</sup> cations near the

perimeter of the metal particles.

For HDO of anisole, demethylation reaction with the production of phenol and methane is the preferred route over Pd/SiO<sub>2</sub>. The demethoxylation reaction producing benzene and methanol is favoured over Pd/Nb<sub>2</sub>O<sub>5</sub> catalyst. In this case, the cleavage of the C<sub>aryl</sub>–O bond is promoted by the oxophilic sites of the support (Nb<sup>4+</sup>/Nb<sup>5+</sup> cations). For Pd/NbOPO<sub>4</sub> catalyst, the high selectivity to phenol is attributed to the acid sites of the support as determined by NH<sub>3</sub>-TPD, which promotes the scission of the C–O bond of the methoxy group.

Phenol and methanol were the main products formed for the HDO of guaiacol, even for the niobia supported catalyst. This result reveals that the presence of both functional groups on the aromatic ring strongly affects the deoxygenation activity of the Pd/Nb<sub>2</sub>O<sub>5</sub> catalyst. In this case, the guaiacol molecule adsorbs through the oxygen atom of methoxy group, followed by the demethoxylation and the formation of phenol that rapidly desorbs unreacted.

Pd/SiO<sub>2</sub>, Pd/Nb<sub>2</sub>O<sub>5</sub>, and Pd/NbOPO<sub>4</sub> catalysts were tested for HDO of pine pyrolysis vapors. In comparison to the non-catalytic experiment, the presence of catalyst reduced the total yield of oxygenated compounds. However, the extent of deoxygenation depended on the support. Niobia-supported catalysts exhibited the highest reduction in the yields of oxygenates (Pd/Nb<sub>2</sub>O<sub>5</sub>: 59%; Pd/NbOPO<sub>4</sub>: 43%; Pd/SiO<sub>2</sub>: 24%). The higher deoxygenation activity of Pd/Nb<sub>2</sub>O<sub>5</sub> and Pd/NbOPO<sub>4</sub> catalysts is in good agreement with the model compound results and is attributed to the oxophilic sites on the support (Nb<sup>4+</sup>/Nb<sup>5+</sup> cations), which have been previously reported to promote C–O bond scissions by forming strong interactions with oxygenated reactants. The distribution of deoxygenated products also varied depending on the support. The dominant aromatic product over Pd/SiO<sub>2</sub> was benzene, whereas Pd/Nb<sub>2</sub>O<sub>5</sub> and Pd/NbOPO<sub>4</sub> favoured the production of alkylated one and two ring aromatics. Among all the deoxygenated products, the yields of aromatics and olefins were higher than the yield of alkanes over Pd/Nb<sub>2</sub>O<sub>5</sub> and Pd/NbOPO<sub>4</sub>. The results show that Pd/Nb<sub>2</sub>O<sub>5</sub> and Pd/NbOPO<sub>4</sub> are potential catalysts for bio-oil upgrading for the production of fuels.

#### Acknowledgments

Camila A. Teles, Priscilla M. de Souza, Raimundo C. Rabelo-Neto and Fabio Bellot Noronha thanks CAPES and CNPQ for the scholarship received. The group thanks the LNLS for the assigned beamtime at XRD-1 and for the valuable support to perform the in situ XRD studies. This work was also supported by the U.S. Department of Energy's Bioenergy Technologies Office (DOE-BETO) and performed in collaboration with the Chemical Catalysis for Bioenergy Consortium (ChemCatBio), a member of the Energy Materials Network (EMN).

The U.S. Government retains and the publisher, by accepting the article for publication, acknowledges that the U.S. Government retains a nonexclusive, paid up, irrevocable, worldwide license to publish or reproduce the published form of this work, or allow others to do so, for U.S. Government purposes. The views and opinions of the authors expressed herein do not necessarily state or reflect those of the United States Government or any agency thereof. Neither the United States Government nor any agency thereof, nor any of their employees, makes any warranty, expressed or implied, or assumes any legal liability or responsibility for the accuracy, completeness, or usefulness of any information, apparatus, product, or process disclosed, or represents that its use would not infringe privately owned rights.

#### Appendix A. Supplementary data

Supplementary material related to this article can be found, in the online version, at doi:<https://doi.org/10.1016/j.apcatb.2018.06.073>.

## References

- [1] D.A. Ruddy, J.A. Schaidle, J.R. Ferrell, J. Wang, L. Moens, J.E. Hensley, *Green Chem. Rev.* 16 (2014) 454–490.
- [2] M.I. Jahirul, M.G. Rasul, A.A. Chowdhury, N. Aswath, *Energies* 5 (2012) 4952–5001.
- [3] S. Wan, T. Pham, S. Zhang, L. Lobban, D. Resasco, R. Mallinson, *AIChE J.* 59 (7) (2013) 2275–2285.
- [4] C. Mukarakate, J.D. McBrayer, T.J. Evans, S. Budhi, D.J. Robichaud, K. Lisa, J.T. Dam, M.J. Watson, R.M. Baldwin, M.R. Nimlos, *Green. Chem.* 17 (2015) 4217–4227.
- [5] M.W. Nolte, J. Zhang, B.H. Shanks, *Green. Chem.* 18 (2016) 134–138.
- [6] R.M. Braga, D.M.A. Melo, E.V. Sobrinho, J.M.F. Barros, M.A.F. Melo, A.F.M. Carvalho, M.S.B. Fontes, J.C.O. Freitas, *Catal. Today* 279 (2017) 224–232.
- [7] Q. Lu, Y. Zhang, Z. Tang, W.-Z. Li, X.-F. Zhu, *Fuel* 89 (2010) 2096–2103.
- [8] L. Nie, P.M. De-Souza, F.B. Noronha, W. An, T. Sooknoi, D.E. Resasco, *J. Mol. Catal. A: Chem.* 388–389 (2014) 47–55.
- [9] P.M. de Souza, L. Nie, L.E.P. Borges, F.B. Noronha, D.E. Resasco, *Catal. Lett.* 144 (2014) 2005–2011.
- [10] Q. Tan, G. Wang, L. Nie, A. Dinse, C. Buda, J. Shabaker, D.E. Resasco, *ACS Catal.* 5 (2015) 6271–6283.
- [11] M.B. Griffin, G.A. Ferguson, D.A. Ruddy, M.J. Biddy, G.T. Beckham, J.A. Schaidle, *ACS Catal.* 6 (2016) 2715–2727.
- [12] P.M. de Souza, R.C. Rabelo-Neto, L.E.P. Borges, G. Jacobs, B.H. Davis, T. Sooknoi, D.E. Resasco, F.B. Noronha, *ACS Catal.* 5 (2015) 1318–1329.
- [13] P.M. de Souza, R.C. Rabelo-Neto, L.E.P. Borges, G. Jacobs, B.H. Davis, U.M. Graham, D.E. Resasco, F.B. Noronha, *ACS Catal.* 5 (2015) 7385–7398.
- [14] P.M. de Souza, R.C. Rabelo-Neto, L.E.P. Borges, G. Jacobs, B.H. Davis, D.E. Resasco, F.B. Noronha, *ACS Catal.* 7 (2017) 2058–2073.
- [15] C. Newman, X. Zhou, B. Goundie, I.T. Thompson, R.A. Pollock, Z. Ross, M.C. Wheeler, R.W. Meulenberg, R.N. Austin, B.G. Frederick, *App. Catal. A: Gen.* 477 (2014) 64–74.
- [16] P.M. Mortensen, J.-D. Grunwaldt, P.A. Jensen, A. Jensen, *ACS Catal.* 3 (2013) 1774–1785.
- [17] C. Zhao, J. He, A. Lemonidou, X. Li, J. Lercher, *J. Catal.* 280 (2011) 8–16.
- [18] C. Zhao, S. Kasakov, J. He, J. Lercher, *J. Catal.* 296 (2012) 12–23.
- [19] J. He, C. Zhao, J.A. Lercher, *J. Catal.* 309 (2014) 362–375.
- [20] A.J.R. Hensley, Y. Wang, J.-S. McEwen, *ACS Catal.* 5 (2015) 523–536.
- [21] T.N. Phan, Y.-K. Park, I.-G. Lee, C.H. Ko, *App. Catal. A: Gen.* 544 (2017) 84–93.
- [22] T.M. Sankaranarayanan, A. Berenguer, C.O. Hernández, I. Moreno, P. Jana, J.M. Coronado, D.P. Serrano, *Catal. Today* 243 (2015) 163–172.
- [23] Y. Yang, C.O. Hernández, V.A.P. O'Shea, P. Pizarro, J.M. Coronado, D.P. Serrano, *App. Catal. B: Env.* 145 (2014) 91–100.
- [24] L. Nie, B. Peng, X. Zhu, *ChemCatChem* (2018), <https://doi.org/10.1002/cctc.201701413>.
- [25] J. Sun, A.M. Karim, H. Zhang, L. Kovarik, X.S. Li, A.J. Hensley, J.-S. McEwen, Y. Wang, *J. Catal.* 306 (2013) 47–57.
- [26] A.K. Deepa, P.L. Dhepe, *ChemPlusChem* 79 (2014) 1573–1583.
- [27] A.M.G. Carvalho, D.H.C. Araújo, H.F. Canova, C.B. Rodella, S.L. Cuffini, R.N. Costa, R.S. Nunes, *J. Synchrotron Rad.* 23 (2016) 1501506.
- [28] P.P. Silva, F.A. Silva, L.S. Portela, L.V. Mattos, F.B. Noronha, C.E. Hori, *Catal. Today* 107 (2005) 734–740.
- [29] M. Boudart, *Adv. Catal.* 20 (1969) 153–166.
- [30] R.J. Madon, M. Boudart, *Ind. Eng. Chem. Fundam.* 21 (1982) 438–447.
- [31] K. Murugappan, C. Mukarakate, S. Budhi, M. Shetty, M.R. Nimlos, Y. Román-Leshkov, *Green. Chem.* 18 (2016) 5548–5557.
- [32] J. Datka, A.M. Turek, J.M. Jehng, I.E. Wachs, *J. Catal.* 135 (1992) 186–199.
- [33] F.M.T. Mendes, C.A. Perez, R.R. Soares, F.B. Noronha, M. Schmal, *Catal. Today* 78 (2003) 449–458.
- [34] H.N. Pham, Y.J. Pagan-Torres, J.C. Serrano-Luiz, D. Wang, J.A. Dumesic, A.K. Datye, *App. Catal. A: Gen.* 397 (2011) 153–162.
- [35] V.F.A. Lewis, *The Palladium Hydrogen System*, Academic Press, London-New York, 1967.
- [36] F.B. Noronha, M. Schmal, M. Primet, R. Frety, *App. Catal.* 78 (1991) 125–139.
- [37] F.B. Noronha, M. Schmal, B. Morawec, P. Delichère, M. Brun, F. Villain, R. Fréty, *J. Phys. Chem. B* 104 (2000) 5478–5485.
- [38] A.M. Barrios, C.A. Teles, P.M. De-Souza, R.C. Rabelo-Neto, G. Jacobs, B.H. Davis, L.E.P. Borges, F.B. Noronha, *Catal. Today* 302 (2018) 115–124.
- [39] T. Nimmanwudipong, R.C. Runnebaum, K. Tay, D.E. Block, B.C. Gates, *Catal. Lett.* 141 (2011) 1072–1078.
- [40] C.A. Teles, R.C. Rabelo-Neto, J.R. Lima, L.V. Mattos, D.E. Resasco, F.B. Noronha, *Catal. Lett.* 146 (2016) 1848–1857.
- [41] Q. Tan, G. Wang, A. Long, A. Dinse, C. Buda, J. Shabaker, D.E. Resasco, *J. Catal.* 347 (2017) 102–115.
- [42] C.A. Teles, R.C. Rabelo-Neto, G. Jacobs, B.H. Davis, D.E. Resasco, F.B. Noronha, *ChemCatChem* 9 (2017) 2850–2863.
- [43] X. Zhu, L. Nie, L.L. Lobban, R.G. Mallinson, D.E. Resasco, *Energy Fuels* 28 (2014) 4104–4111.
- [44] C.U. Pittman Jr, D. Mohan, A. Eseyin, Q. Li, L. Ingram, E.-B.M. Hassan, B. Mitchell, H. Guo, P.H. Steele, *Energy Fuels* 26 (2012) 3816–3825.
- [45] F.B. Noronha, E.C. Fendley, R.R. Soares, W.E. Alvarez, D.E. Resasco, *Chem. Eng. J.* 82 (2001) 21–31.
- [46] G. Danni, S. Christopher, T.H. Hyun, V. Arving, *Ind. Eng. Chem. Res.* 53 (2014) 18685–18667.
- [47] P. McKendry, *Bioresour. Technol.* 83 (1) (2001) 37–46.
- [48] S. Zhou, Y. Xue, A. Sharma, X. Bai, *ACS Sustain. Chem. Eng.* 4 (2016) 6608–6617.
- [49] R.J. Evans, T.A. Milne, *Energy Fuels* 1 (1987) 123–137.
- [50] G.W. Huber, S. Iborra, A. Corma, *Chem. Rev.* 106 (2006) 4044–4098.
- [51] M.S. Tamaldge, R.M. Baldwin, M.J. Biddy, R.L. McCormic, G.T. Beckham, G.A. Ferguson, S. Czernik, K.A. Magrini-Bair, T.D. Foust, P.D. Metelski, C. Hetrick, M.R. Nimlos, *Green. Chem.* 16 (2014) 407–453.